Quantum hydrogen-bond symmetrization in the superconducting hydrogen sulfide system

Ion Errea[1,2], Matteo Calandra[3], Chris J. Pickard[4], Joseph R. Nelson[5], Richard J. Needs[5], Yinwei Li[6], Hanyu Liu[7], Yunwei Zhang[8], Yanming Ma[8], and Francesco Mauri[3,9]
[1]*Fisika Aplikatua 1 Saila, EUITI Bilbao, University of the Basque Country (UPV/EHU), Rafael Moreno "Pitxitxi" Pasealekua 3, 48013 Bilbao, Basque Country, Spain*
[2]*Donostia International Physics Center (DIPC), Manuel Lardizabal pasealekua 4, 20018 Donostia/San Sebastián, Basque Country, Spain*
[3]*IMPMC, UMR CNRS 7590, Sorbonne Universités - UPMC Univ. Paris 06, MNHN, IRD, 4 Place Jussieu, F-75005 Paris, France*
[4] *Department of Materials Science & Metallurgy, University of Cambridge, 27 Charles Babbage Road, Cambridge CB3 0FS, UK*
[5]*Theory of Condensed Matter Group, Cavendish Laboratory, J J Thomson Avenue, Cambridge CB3 0HE, UK*
[6]*School of Physics and Electronic Engineering, Jiangsu Normal University, Xuzhou 221116, People's Republic of China*
[7] *Geophysical Laboratory, Carnegie Institution of Washington, Washington D.C. 20015, USA*
[8]*State Key Laboratory of Superhard Materials, Jilin University, Changchun 130012, People's Republic of China and*
[9] *Dipartimento di Fisica, Università di Roma La Sapienza, Piazzale Aldo Moro 5, I-00185 Roma, Italy*

Hydrogen compounds are peculiar in that the quantum nature of the proton can crucially affect their structural and physical properties. A remarkable example is the high-pressure phases [1, 2] of H_2O, where quantum proton fluctuations favor symmetrization of the H bond and lower by 30 GPa the boundary between asymmetric and symmetric structures [3]. Here we show that an analogous quantum symmetrization occurs in the recently discovered [4] sulfur hydride superconductor with a record superconducting critical temperature $T_c = 203$ K at 155 GPa. Superconductivity occurs via formation of a structure of stoichiometry H_3S with S atoms arranged on a body-centered-cubic (bcc) lattice [5–9]. If the H atoms are treated as classical particles, then for $P \gtrsim 175$ GPa they are predicted to sit midway between two S atoms in a structure with $Im\bar{3}m$ symmetry. At lower pressures the H atoms move to an off-center position forming a short H−S covalent bond and a longer H···S hydrogen bond in a structure with $R3m$ symmetry [5–9]. X-ray diffraction experiments confirmed the H_3S stoichiometry and the S lattice sites, but were unable to discriminate between the two phases [10]. Our present *ab initio* density-functional theory (DFT) calculations show that quantum nuclear motion lowers the symmetrization pressure by 72 GPa for H_3S and by 60 GPa for D_3S. Consequently, we predict that the $Im\bar{3}m$ phase dominates the pressure range within which a high T_c was measured. The observed pressure-dependence of T_c is closely reproduced in our calculations for the $Im\bar{3}m$ phase, but not for the $R3m$ phase. Thus, the quantum nature of the proton fundamentally changes the superconducting phase diagram of H_3S.

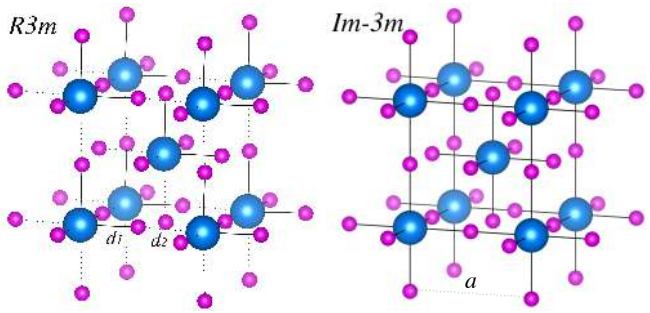

FIG. 1. **Crystal structures of the competing phases.** Crystal structure in the conventional bcc cell of the $R3m$ and $Im\bar{3}m$ phases. In the $R3m$ structure the H−S covalent bond of length d_1 is marked with a solid line and the longer H···S hydrogen bond of length d_2 with a dotted line. In the $Im\bar{3}m$ phase $d_1 = d_2$. In the $Im\bar{3}m$ structure we mark the lattice paramerter a.

The discovery of high-temperature superconductivity in compressed hydrogen sulfide [4] has generated intense interest over the last year, and has led to a number of theoretical studies aimed at understanding the phase diagram of the H-S system as well as the origin of the astonishingly high T_c observed [5–9, 12–18]. The overall consensus is that H_2S, the only stable compound formed by hydrogen and sulfur at ambient conditions, is metastable at high pressures and its decomposition gives rise to several H-S compounds. High-T_c superconductivity is believed to occur in a structure of H_3S stoichiometry, and is considered to be conventional in nature, i.e., mediated by electron-phonon interactions [4, 5, 7, 9, 12–17]. Alternatives to conventional superconductivity have also been

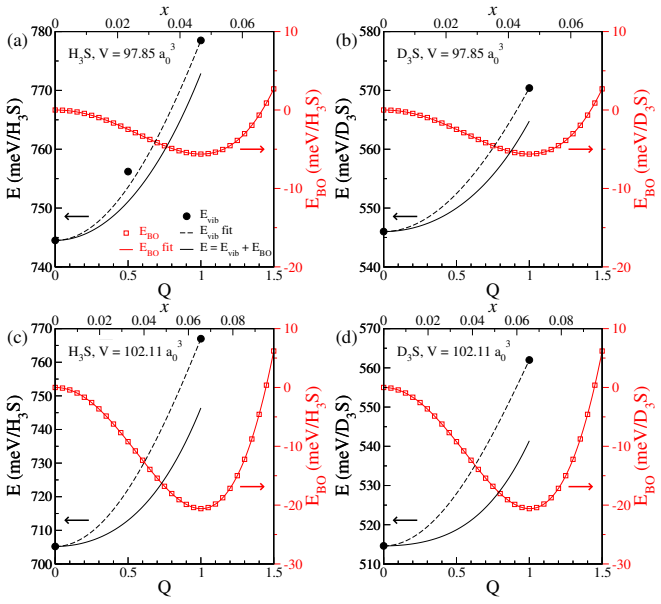

FIG. 2. **Energetics.** $E_{\rm BO}$, $E_{\rm vib}$, and $E = E_{\rm vib} + E_{\rm BO}$ curves are shown as a function of the reaction coordinate Q that transforms the $Im\bar{3}m$ structure ($Q = 0$) into the $R3m$ structure ($Q = 1$), as well as the relative coordinate x that measures the off-centering of the H atoms, defined as $x = (d_2 - a/2)/(a/2)$, where d_2 is the length of the hydrogen bond and a the lattice parameter (see Fig. 1). The left-hand axes show the energy scale for $E_{\rm vib}$ and E, and the right-hand axes show the scale for $E_{\rm BO}$. Crystal symmetry implies that $E(Q) = E(-Q)$, so that the curves can be fitted to polynomials with only even terms. This guarantees that the transition is second-order according to Landau theory [11]. Results are presented for two different volumes of the primitive bcc lattice; $V = 97.85a_0^3$ corresponds to approximately 150 GPa and $V = 102.11a_0^3$ to 130 GPa. The pressure associated with each volume depends on both the isotope and Q (see Extended Data for the equations of states). Black circles represent calculated $E_{\rm vib}$ points and the black dashed line the fitted $E_{\rm vib}(Q)$ curve (see Methods). The $E(Q)$ curve is obtained by addition of the fitted $E_{\rm vib}$ and $E_{\rm BO}$ curves.

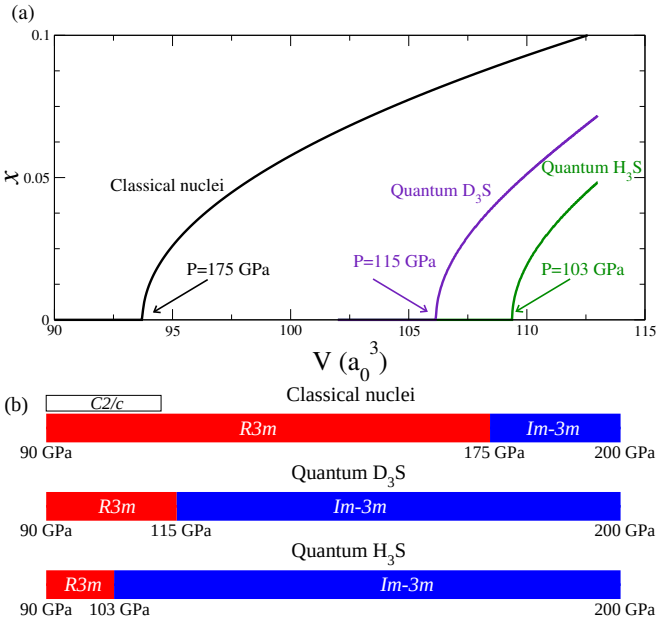

FIG. 3. **Second-order phase transition.** (a) For each volume we plot the relative coordinate x that yields the minimum total energy. x measures the off-centering of the H atoms (see caption of Fig. 2). The results are shown in the classical nuclei limit, as well as in the quantum case both for H_3S and D_3S. The volume at which x departs from zero marks the second-order phase transition from the $Im\bar{3}m$ phase to $R3m$ phase. Transition pressures are also indicated, which include the effects of vibrational energies. (b) Phase diagram for the second-order phase transition as a function of pressure. As shown in Ref. 8, below 112 GPa H_3S adopts a very different $C2/c$ phase. We mark the expected emergence of this phase by a box.

discussed [18]. According to structural predictions [5–9], H_3S adopts a rhombohedral $R3m$ form between approximately 112 and 175 GPa, and a cubic $Im\bar{3}m$ at higher pressures. As shown in Fig. 1, the $R3m$ phase is characterized by covalently bonded SH_3 units with a covalent H−S bond of length d_1. Each of these H atoms is bonded to the next S atom by a hydrogen H···S bond of length d_2. The $Im\bar{3}m$ phase, in contrast, has full cubic symmetry, with $d_1 = d_2$ so that each H atom resides midway between the two S atoms, as shown in Fig. 1. The $R3m$ structure is nevertheless very close to cubic symmetry, for example, the DFT-relaxed $R3m$ structure, which represents the minimum of the Born-Oppenheimer energy surface (BOES), has a rhombohedral angle of 109.49° at ≈150 GPa, compared to 109.47° for a perfect bcc lattice. We have verified that imposing a cubic angle on the $R3m$ structure has a negligible effect on the energy difference between the $R3m$ and $Im\bar{3}m$ structures. Consequently, we assume a cubic lattice for both phases in the following.

The bond-symmetrizing second-order transition from $R3m$ to $Im\bar{3}m$ occurs at 175 GPa according to our static lattice calculations. At this pressure, our harmonic phonon calculations show that a Γ-point optical phonon of the high-symmetry $Im\bar{3}m$ phase becomes imaginary, implying that $Im\bar{3}m$ is at a saddle point of the BOES between 112 and 175 GPa, while the $R3m$ phase lies at the minimum. Crystal symmetry guarantees that the transition is of second-order type (see Extended Data for a symmetry analysis). As occurs in the high-pressure ice X phase [3, 19, 20] and other hydrogenated compounds [21], the quantum nature of the proton can radically alter the pressure at which the second-order phase transition occurs and, in the present case, can strongly affect the stability of the $R3m$ phase below 175 GPa. Determining the stability ranges of these phases therefore requires the inclusion of vibrational zero-point energy (ZPE) alongside the static BOES energy. However, the presence of imaginary phonon frequencies hinders calculations of

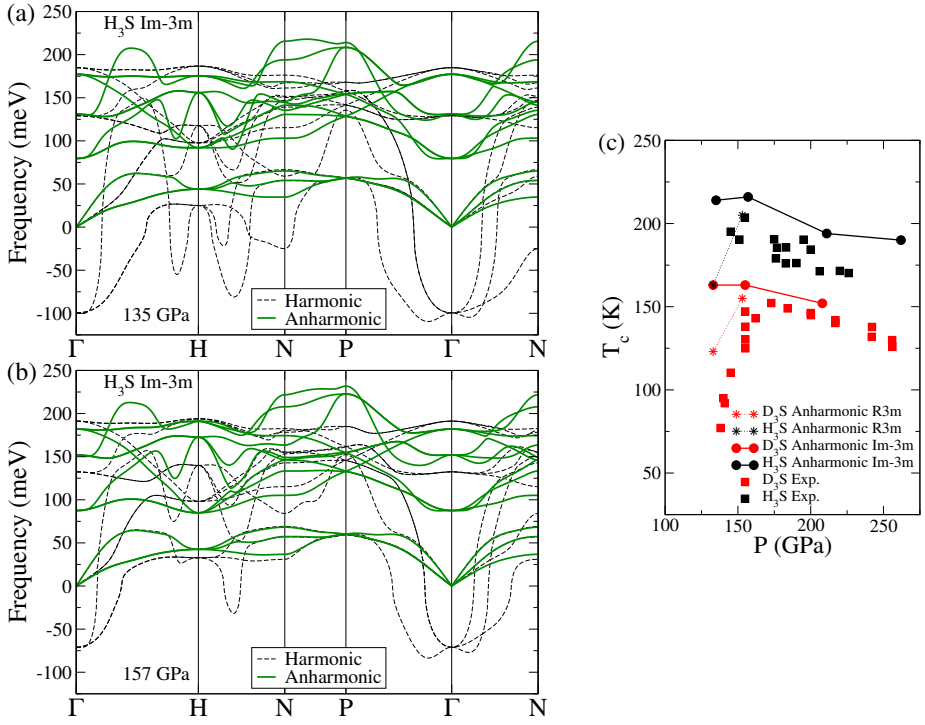

FIG. 4. **Phonon spectra and superconducting critical temperature.** Harmonic and SSCHA anharmonic phonon spectra of the cubic high-symmetry $Im\bar{3}m$ structure for H_3S at different pressures: (a) 135 GPa and (b) 157 GPa. (c) Superconducting T_c's calculated with the anharmonic phonons for the $Im\bar{3}m$ structure compared with experimental results obtained after annealing [4]. T_c results obtained with anharmonic phonons for the $R3m$ structure below 175 GPa are also shown. Each pressure takes the vibrational energy into account.

the ZPE, since the quasi-harmonic approximation breaks down, and anharmonicity becomes a crucial ingredient.

To elucidate the role of anharmonicity and quantum effects in the pressure range in which the record T_c was observed, we make use of the stochastic self-consistent harmonic approximation (SSCHA) [22, 23]. The variational SSCHA method was devised for calculating the free energy and phonon spectra while fully incorporating quantum and anharmonic effects, and it is therefore perfectly suited for our purpose. All of the calculations presented here are performed at 0 K. Primitive cells for the $R3m$ and $Im\bar{3}m$ structures contain 4 atoms (1 S atom and 3 H atoms), and therefore a particular nuclear configuration can be described by a 12-dimensional vector $\mathbf{R}$ containing the atomic coordinates. In the classical limit the ZPE is neglected and the energy of a nuclear configuration $\mathbf{R}$ is given by the DFT Born-Oppenheimer energy $E_{\rm BO}(\mathbf{R})$. In the SSCHA, the ZPE is accounted for by approximating the nuclear wave-function by a Gaussian centered on a centroid coordinate $\mathbf{R}_{\rm c}$, which denotes the average and most probable position of the nuclei. For a given $\mathbf{R}_{\rm c}$, the width of the Gaussian is obtained by a variational minimization of the expectation value of the sum of the nuclear potential and kinetic energies. In the following analysis it is convenient to split the SSCHA total energy $E(\mathbf{R}_{\rm c})$ into static and anharmonic-vibrational-ZPE contributions: $E(\mathbf{R}_{\rm c}) = E_{\rm BO}(\mathbf{R}_{\rm c}) + E_{\rm vib}(\mathbf{R}_{\rm c})$.

We study the energy landscape $E(\mathbf{R}_{\rm c})$ along the line defined by $\mathbf{R}_{\rm c}(Q) = \mathbf{R}_{Im\bar{3}m} + Q(\mathbf{R}_{R3m} - \mathbf{R}_{Im\bar{3}m})$, where $\mathbf{R}_{Im\bar{3}m}$ and $\mathbf{R}_{R3m}$ are, respectively, the coordinates corresponding to the saddle point and minimum of the BOES, representing the two different symmetries. Here, Q is a real number describing the reaction coordinate, so that at $Q = 0$ the centroids are located at the atomic positions of $Im\bar{3}m$, and at $Q = 1$ at the atomic positions of $R3m$. Hence, Q measures the off-centering of the hydrogen nuclear wave-function and can be associated with the relative coordinate $x = (d_2 - a/2)/(a/2)$ that quantifies the length of the H$\cdots$S hydrogen bond with respect to the symmetric position (a is the lattice parameter). We analyze the curve $E(\mathbf{R}_{\rm c}(Q)) \equiv E(Q)$ for a fixed primitive bcc unit cell. As shown in Fig. 2(a) for a cell volume of $97.85a_0^3$ the $E_{\rm BO}(Q)$ curve has a shallow double-well structure favoring the $R3m$ structure by only 5.6 meV/H_3S. However, after adding the $E_{\rm vib}(Q)$ energy calculated with the SSCHA, the full $E(Q)$ curve shows a clear minimum at $Q = 0$, which favors the $Im\bar{3}m$ structure. At a larger volume of 102.11 a_0^3, which corresponds to a pressure of around 130 GPa, the minimum of $E(Q)$ is also at $Q = 0$, despite the fact that the one-dimensional Born-Oppenheimer well in $E_{\rm BO}(Q)$ becomes deeper, as shown in Fig. 2(c). Repeating these calcula-

tions for D_3S, we find that the $Im\bar{3}m$ structure is the most favorable once the ZPE has been included. We therefore conclude that the quantum nature of the nuclei symmetrizes the hydrogen bond and leads to a proton wave-function centered at the atomic positions of $Im\bar{3}m$ for both H_3S and D_3S. To eliminate the possibility that the energy minimum occurs beyond the $\mathbf{R}_c(Q)$ line studied, we performed an unconstrained SSCHA minimization, optimizing both the width of the Gaussians and the $\mathbf{R}_c$ centroid positions. The results of this minimization show again that, within stochastic error, the centroid position obtained corresponds to the $Im\bar{3}m$ structure, in which the H−S covalent and H$\cdots$S hydrogen bond distances equalize, leading to symmetric hydrogen bonds.

The difference between the vibrational energies of $R3m$ and $Im\bar{3}m$ as a function of the x coordinate is weakly dependent on volume. This allows us to interpolate $E(x)$ in a wide volume range and estimate the pressure at which the proton wave-function shifts away from the centered position. Our calculations show that this symmetry breaking occurs at 103 GPa in H_3S and 115 GPa in D_3S (see Fig. 3). The higher transition pressure in D_3S is due to weaker quantum effects. This isotope effect is similar to the one observed in the ice VII/ice X transition [24]. Considering that below 112 GPa the $R3m$ phase is expected to transform into a very different $C2/c$ phase consisting of isolated H_2S and H_2 molecules with H_3S stoichiometry [8], $R3m$-H_3S might not be formed. However, D_3S may adopt the $R3m$ structure at pressures below the transition to the $Im\bar{3}m$ phase.

The quantum proton symmetrization has an enormous impact on the phonon spectra of H_3S. As mentioned earlier, and shown in Fig. 4, the phonon spectra of $Im\bar{3}m$-H_3S have several imaginary modes in the harmonic approximation below 175 GPa. The corresponding anharmonic SSCHA phonon spectra for $Im\bar{3}m$-H_3S show well-behaved phonon dispersion relations with positive frequencies in the pressure range of interest (Fig. 4). This is analogous to ice X, which has only real positive phonon frequencies once the classical limit predicts symmetrization of the hydrogen bond [25–28]. The anharmonic renormalization of the phonon energies is huge, especially for the H-S bond-stretching modes in which H atoms move towards the neighboring S atoms, which are precisely those modes which drive the second-order phase transition between the $Im\bar{3}m$ and $R3m$ phases. Therefore, the proximity to the second-order quantum phase transition is the origin of the strong anharmonicity.

While the bond symmetrization in ice X occurs in an insulating system, H_3S is metallic and the symmetrization strongly affects the superconductivity. Indeed, the calculated electron-phonon coupling and superconducting T_c lend further support to the suggestion that $Im\bar{3}m$-H_3S yields the record T_c. We use Wannier interpolated electron-phonon matrix elements in our calculations [29] and estimate T_c solving the isotropic Migdal-Eliashberg equations. The phonon frequencies and polarizations that enter the electron-phonon calculations are calculated using the SSCHA. Thus, in the present treatment we neglect non-linear corrections of the electron-phonon vertices and non-adiabatic effects that could arise from the small mass of H. The results obtained for the $Im\bar{3}m$ structure using anharmonic phonon frequencies agree well with experimental measurements of T_c for H_3S and D_3S and correctly capture the observed increase in T_c with decreasing pressure. We also find an isotope coefficient $\alpha = -[\ln T_c(D_3S) - \ln T_c(H_3S)]/\ln 2$ for H→D substitution of $\alpha = 0.35$ at 210 GPa and $\alpha = 0.40$ at 155 GPa in good agreement with experiment (see Fig. 4(c)). The electron-phonon coupling constant λ, which scales with the phonon frequencies as $\propto 1/\omega^2$, is enhanced with decreasing pressure due to the overall softening of the phonon modes. This explains the smooth decrease of T_c with increasing pressure. Between approximately 130 and 150 GPa the increase in λ is compensated by the decrease in the average phonon frequency and T_c saturates. We also present SSCHA calculations for the $R3m$ structure keeping the centroids at the $Q = 1$ position. We find a rapid drop in T_c with decreasing pressure as in previous harmonic calculations [13]. Therefore, the observed high-T_c superconductivity cannot be explained by H_3S in the $R3m$ phase, although the sudden drop in T_c measured for D_3S below 150 GPa [4] could be an indication of the symmetry breaking that we predicted at 115 GPa. Indeed, the predicted transition pressure depends on the choice of the exchange correlation functional (see Methods). Even if our choice of the PBE exchange-correlation functional [30] appears appropriate, based on agreement between the experimentally observed equation of state [10] and DFT calculations, we cannot exclude a small error in the transition pressure. However, the isotopic shift of the transition pressure is independent of the functional. Thus, if the drop in T_c observed experimentally in D_3S is due to the transition from $R3m$ to $Im\bar{3}m$, we predict that a similar drop also occurs in H_3S but is shifted to lower pressures by about 12 GPa. Considering that the $Im\bar{3}m$ phase has no Raman active modes, if the drop in T_c in D_3S coincides with the second-order phase transition, we predict that Raman peaks from the $R3m$ phase would emerge at that pressure.

The recent experiment by Drozdov *et al.* [4] suggests that room-temperature superconductivity is reachable in other hydrogen-rich compounds. Our results show that in such hydrogen-rich materials with prospects for high-T_c superconductivity the quantum motion of the proton induces non-trivial effects that strongly affect the thermodynamical stability, the hydrogen chemical bonding, and the electron-phonon coupling strength.

Online Content See Methods and Extended Data items in the online version of the paper for a symmetry analysis of the phase transition, calculations with different exchange-correlation functionals, the equations

of state, harmonic and anharmonic phonon spectra of $Im\bar{3}m$-D_3S, anharmonic phonon spectra of the $R3m$ phase, and superconducting properties of both the $Im\bar{3}m$ and $R3m$ structures.

[1] Goncharov, A. F., Struzhkin, V. V., Somayazulu, M. S., Hemley, R. J. & Mao, H. K. Compression of ice to 210 gigapascals: Infrared evidence for a symmetric hydrogen-bonded phase. *Science* **273**, 218–220 (1996).

[2] Loubeyre, P., LeToullec, R., Wolanin, E., Hanfland, M. & Hausermann, D. Modulated phases and proton centring in ice observed by x-ray diffraction up to 170 GPa. *Nature* **397**, 503–506 (1999).

[3] Benoit, M., Marx, D. & Parrinello, M. Tunnelling and zero-point motion in high-pressure ice. *Nature* **392**, 258–261 (1998).

[4] Drozdov, A. P., Eremets, M. I., Troyan, I. A., Ksenofontov, V. & Shylin, S. I. Conventional superconductivity at 203 kelvin at high pressures in the sulfur hydride system. *Nature* **525**, 73–76 (2015).

[5] Duan, D., Liu, Y., Tian, F., Li, D., Huang, X., Zhao, Z. Yu, H., Liu, B., Tian, W. & Cui, T. Pressure-induced metallization of dense $(H_2S)_2H_2$ with high-Tc superconductivity. *Sci. Rep.* **4**, 6968 (2014).

[6] Duan, D., Huang, X., Tian, F., Li, D., Yu, H., Liu, Y., Ma, Y., Liu, B. & Cui, T. Pressure-induced decomposition of solid hydrogen sulfide. *Phys. Rev. B* **91**, 180502 (2015).

[7] Errea, I., Calandra, M., Pickard, C. J., Nelson, J. R., Needs, R. J., Li, Y., Liu, H., Zhang, Y., Ma, Y. & Mauri, F. High-pressure hydrogen sulfide from first principles: A strongly anharmonic phonon-mediated superconductor. *Phys. Rev. Lett.* **114**, 157004 (2015).

[8] Li, Y., Wang, L., Liu, H., Zhang, Y., Hao, J., Pickard, C. J., Nelson, J. R., Needs, R. J., Li, W., Huang, Y., Errea, I., Calandra, M., Mauri, F. & Ma, Y. Dissociation products and structures of solid H_2S at strong compression. *Phys. Rev. B* **93**, 020103(R) (2016).

[9] Bernstein, N., Hellberg, C. S., Johannes, M. D., Mazin, I. I. & Mehl, M. J. What superconducts in sulfur hydrides under pressure and why. *Phys. Rev. B* **91**, 060511 (2015).

[10] Einaga, M., Sakata, M., Ishikawa, T., Shimizu, K., Eremets, M. I., Drozdov, A. P., Troyan, I. A., Hirao, N. & Ohishi, Y. Crystal Structure of 200 K-Superconducting Phase of Sulfur Hydride System. *ArXiv e-prints*, arXiv:1509.03156 (2015).

[11] Landau, L. D. & Lifshitz, E. M. *Course of Theoretical Physics*, volume 5 Statistical Physics. Butterworth-Heinemann, 3rd edition (1980).

[12] Papaconstantopoulos, D. A., Klein, B. M., Mehl, M. J. & Pickett, W. E. Cubic H_3S around 200 GPa: An atomic hydrogen superconductor stabilized by sulfur. *Phys. Rev. B* **91**, 184511 (2015).

[13] Akashi, R., Kawamura, M., Tsuneyuki, S., Nomura, Y. & Arita, R. First-principles study of the pressure and crystal-structure dependences of the superconducting transition temperature in compressed sulfur hydrides. *Phys. Rev. B* **91**, 224513 (2015).

[14] Nicol, E. J. & Carbotte, J. P. Comparison of pressurized sulfur hydride with conventional superconductors. *Phys. Rev. B* **91**, 220507 (2015).

[15] Flores-Livas, J. A., Sanna, A. & Gross, E. K. U. High temperature superconductivity in sulfur and selenium hydrides at high pressure. *ArXiv e-prints*, arXiv:1501.06336 (2015).

[16] Li, Y., Hao, J., Liu, H., Li, Y. & Ma, Y. The metallization and superconductivity of dense hydrogen sulfide. *The Journal of Chemical Physics* **140**, 174712 (2014).

[17] Bianconi, A. & Jarlborg, T. Superconductivity above the lowest earth temperature in pressurized sulfur hydride. *EPL (Europhysics Letters)* **112**, 37001 (2015).

[18] Hirsch, J. E. & Marsiglio, F. Hole superconductivity in H_2S and other sulfides under high pressure. *Physica C: Superconductivity and its Applications* **511**, 45–49 (2015).

[19] Lee, C., Vanderbilt, D., Laasonen, K., Car, R. & Parrinello, M. *Ab initio* studies on high pressure phases of ice. *Phys. Rev. Lett.* **69**, 462–465 (1992).

[20] Lee, C., Vanderbilt, D., Laasonen, K., Car, R. & Parrinello, M. *Ab initio* studies on the structural and dynamical properties of ice. *Phys. Rev. B* **47**, 4863–4872 (1993).

[21] McMahon, M. I., Nelmes, R. J., Kuhst, W. F., Dorwarth, R., Piltz, R. O. & Tun, Z. Geometric effects of deuteration on hydrogen-ordering phase transitions. *Nature* **348**, 317–319 (1990).

[22] Errea, I., Calandra, M. & Mauri, F. First-principles theory of anharmonicity and the inverse isotope effect in superconducting palladium-hydride compounds. *Phys. Rev. Lett.* **111**, 177002 (2013).

[23] Errea, I., Calandra, M. & Mauri, F. Anharmonic free energies and phonon dispersions from the stochastic self-consistent harmonic approximation: Application to platinum and palladium hydrides. *Phys. Rev. B* **89**, 064302 (2014).

[24] Song, M., Yamawaki, H., Fujihisa, H., Sakashita, M. & Aoki, K. Infrared investigation on ice VIII and the phase diagram of dense ices. *Phys. Rev. B* **68**, 014106 (2003).

[25] Goncharov, A. F., Struzhkin, V. V., Mao, H. K. & Hemley, R. J. Raman spectroscopy of dense H_2O and the transition to symmetric hydrogen bonds. *Phys. Rev. Lett.* **83**, 1998 (1999).

[26] Caracas, R. Dynamical instabilities of ice X. *Phys. Rev. Lett.* **101**, 085502 (2008).

[27] Marqués, M., Ackland, G. J. & Loveday, J. S. Nature and stability of ice X. *High Pressure Research* **29**, 208–211 (2009).

[28] Bronstein, Y., Depondt, P., Finocchi, F. & Saitta, A. M. Quantum-driven phase transition in ice described via an efficient langevin approach. *Phys. Rev. B* **89**, 214101 (2014).

[29] Calandra, M., Profeta, G. & Mauri, F. Adiabatic and nonadiabatic phonon dispersion in a wannier function approach. *Phys. Rev. B* **82**, 165111 (2010).

[30] Perdew, J. P., Burke, K. & Ernzerhof, M. Generalized gradient approximation made simple. *Phys. Rev. Lett.* **77**, 3865–3868 (1996).

Acknowledgements We acknowledge financial support from the Spanish Ministry of Economy and Competitiveness (FIS2013- 48286-C2-2-P), French Agence Nationale de la Recherche (Grant No. ANR-13-IS10-0003-01), EPSRC (UK) (Grant No. EP/J017639/1), Cambridge Commonwealth Trust, National Natural Science Foundation of China (Grants No. 11204111, 11404148,

and 11274136), and 2012 Changjiang Scholars Program of China. Work at Carnegie was supported by EFree, an Energy Frontier Research Center funded by the DOE, Office of Science, Basic Energy Sciences under Award No. DE-SC-0001057. Computer facilities were provided by the PRACE project AESFT and the Donostia International Physics Center (DIPC).

Author Contributions I.E., M.C., and F.M. performed the anharmonic and superconducting calculations. All authors contributed to the design of the research project and to the writing of the manuscript.

Author Information The authors declare no competing financial interests. Correspondence and requests for materials should be addressed to I.E. (ion.errea@ehu.eus), M.C (matteo.calandra@impmc.upmc.fr), and F.M. (francesco.mauri@uniroma1.it).

METHODS

Calculation Details Supercell calculations for the SSCHA [22, 23] and linear response calculations [31] were performed within DFT and the generalized gradient approximation functional [30] as implemented in the QUANTUM ESPRESSO [32] code. We used ultrasoft pseudopotentials [33], a plane-wave cutoff energy of 60 Ry for the kinetic energy and 600 Ry for the charge density. The charge density and dynamical matrices were calculated using a 32×32×32 Monkhorst-Pack shifted electron-momentum grid for the unit cell calculations. This mesh was adjusted accordingly in the supercell calculations. The electron-phonon coupling was calculated by using electron and phonon momentum grids composed of up to 42×42×42 randomly displaced points in the Brillouin zone. The isotropic Migdal-Eliashberg equations were solved using 512 Matsubara frequencies and $\mu^* = 0.16$.

The SSCHA calculations were performed using a 3×3×3 supercell for both H_3S and D_3S in the $Im\bar{3}m$ phase, yielding dynamical matrices on a commensurate 3×3×3 q-point grid. The difference between the harmonic and anharmonic dynamical matrices in the 3×3×3 phonon momentum grid was interpolated to a 6×6×6 grid. Adding the harmonic matrices to the result, the anharmonic dynamical matrices were obtained on a 6×6×6 grid. These dynamical matrices were used for the anharmonic electron-phonon coupling calculation. The SSCHA calculations for $Q = 1$ were performed with a 2×2×2 supercell. For consistency, the vibrational energies presented in Fig. 2 were also calculated using a 2×2×2 supercell. The electron-phonon calculations for $Q = 1$ were, however, performed with the SSCHA dynamical matrices interpolated to a 6×6×6 grid from the 2×2×2 mesh.

The $E_{\rm vib}(Q)$ curves in Fig. 2 were obtained as follows. $E_{\rm vib}$ was calculated for $Q = 0$ and $Q = 1$ with the SSCHA. With the SSCHA calculation at $Q = 1$, we extracted $\frac{\mathrm{d}E_{\rm vib}}{\mathrm{d}Q}(Q = 1)$ with no further computational effort. Considering that the derivative of the curve at $Q = 0$ vanishes by symmetry, we can obtain straightforwardly a potential of the form $E_{\rm vib}(Q) = A+BQ^2+CQ^4$. The $E_{\rm vib}$ fit curves presented in Fig. 2 were obtained in this way. The extra point obtained at $Q = 0.5$ for H_3S at $V = 97.85a_0^3$ (see Fig. 2(a)) confirmed the validity of the fitting procedure. The $E_{\rm BO}(Q)$ BOES energies were calculated for many Q points yielding an accurate fitting curve. Fig. 3 was obtained using a polynomial interpolation of the BOES in the volume range shown and adding the $E_{\rm vib}^{R3m} - E_{\rm vib}^{Im\bar{3}m}(x)$ curves that are practically independent of volume.

Symmetry analysis of the second-order phase transition The bond-symmetrization transition from $R3m$ to $Im\bar{3}m$ is a second-order transition and is driven by the softening of an optical mode at Γ. The mode driving the transition belongs to the irreducible representation T_{1u}, also denoted as Γ_4^-, whose dimension is 3 [34, 35]. This irreducible representation is compatible with a group-subgroup relation between the $Im\bar{3}m$ and $R3m$ space groups. As the mode driving the transition is at the Γ point, the transition occurs without increasing the unit cell size, which contains four atoms in the primitive cell of the bcc lattice of the $Im\bar{3}m$ structure as well as in the rhombohedral lattice of the $R3m$ phase.

In a transition from the $m\bar{3}m$ (O_h) point group to the $3m$ (C_{3v}), the most general free energy expansion only contains even terms of the order parameters [36]. Therefore, according to Landau theory [11], the transition must be of second-order. Our reaction coordinate Q used to describe the second-order transition is a simplified order parameter. The fact that $E(Q) = E(-Q)$ confirms that the transition is of second-order.

Equations of state In Extended Data Fig. 1 we present the equation of state both for the $Im\bar{3}m$ and $R3m$ phases. The pressure is calculated both with and without the vibrational contribution to the energy, for H_3S and D_3S. The latter curves are used to include the vibrational effects on the calculated pressures. The vibrational energy calculated includes anharmonicity in all cases as calculated by the SSCHA. The vibrational energy has a small contribution to the calculated pressure, which varies slightly with the isotopic mass. The $P(V)$ curve can be efficiently fitted to the third-order Birch-Murnaghan equation. The parameters of the fit are given in Extended Data Table I.

Dependence on the exchange-correlation functional All calculations presented in the manuscript are calculated within the generalized gradient approximation (GGA) under the PBE parametrization [30]. However, we have performed additional calculations within the local density approximation (LDA) [37] and the BLYP [38, 39] parametrization of the GGA. The second order phase transition at the static level from $Im\bar{3}m$ to $R3m$, which occurs at 175 GPa within PBE, is reduced to 145 GPa in the LDA and increased to 257 GPa with the BLYP parametrization. In Extended Data Fig. 2 we compare the relative coordinate $x = (d_2-a/2)/(a/2)$ as a function of volume, where d_2 is the length of the hydrogen bond and a is the lattice parameter. The x coordinate is obtained both with the static BOES energy $E_{\rm BO}$ as well as with the total energy $E = E_{\rm BO} + E_{\rm vib}$. The vibrational energy is however assumed to be independent of the functional, and the value obtained with PBE is used for estimating $E_{\rm vib}$ for both LDA and BLYP. We believe this is justified because the differences between the vibrational energies of $Im\bar{3}m$ and $R3m$ calculated within the SSCHA and using PBE are very weakly volume dependent as shown in Extended Data Fig. 4. At the static level, the LDA symmetrizes the structure at a pressure 30 GPa below PBE, while BLYP symmetrizes

it at a pressure 82 GPa above PBE. When including the vibrational contribution as described above, the transition between $Im\bar{3}m$ and $R3m$ occurs at 170 GPa for H_3S and 185 GPa for D_3S within BLYP. The shift of the transition pressure induced by the zero-point energy and its isotope dependence is similar for PBE and BLYP. The fully symmetric $Im\bar{3}m$ H_3S structure is always favoured within the LDA for H_3S over the pressure range studied, and it only becomes unfavorable below 89 GPa for D_3S.

Although the choice of exchange-correlation functional adds some uncertainty to the predicted transition pressure, we believe PBE is the most appropriate choice. This statement is based on the fact that PBE best reproduces the experimental equation of state results of Einaga *et al.* [10]. BLYP overestimates the volume, specially when the vibrational contribution is considered (see Extended Data Fig. 3). Indeed, it is well known that BLYP vastly overestimates the equilibrium volumes in metals [40] and, therefore, it is not the best choice for H_3S. On the contrary, when including the vibrational contribution to the pressure, which is calculated in all cases using the PBE functional, the PBE equation of state is in rather good agreement with experimental results [10] and certainly performs better than LDA and BLYP.

Phonons of $Im\bar{3}m$-D_3S In Extended Data Fig. 5 we show the harmonic and anharmonic phonon spectra of D_3S in the $Im\bar{3}m$ phase at two different pressures.

Anharmonic phonon dispersion in the $R3m$ phase In Extended Data Fig. 6 we show the SSCHA phonon spectra calculated for the $R3m$ phase at two different pressures. Here the centroid position of the SSCHA is placed at the minimum of the BOES, which is not a minimum of the total energy as discussed in the manuscript. The Raman active modes of the $R3m$ phase are listed in Extended Data Table II.

Superconducting properties In Extended Data Table III we summarize the calculated values of the electron-phonon coupling constant λ, logarithmic frequency average $\omega_{\log}$, and superconducting T_c.

In Extended Data Fig. 7 we show the Eliashberg function $\alpha^2F(\omega)$ and integrated electron-phonon coupling constant $\lambda(\omega)$ of the $Im\bar{3}m$ phase at two different pressures calculated using the SSCHA phonons. The $\alpha^2F(\omega)$ in the anharmonic case for the $R3m$ structure is given in Extended Data Fig. 6.

[31] Baroni, S., de Gironcoli, S., Dal Corso, A. & Giannozzi, P. Phonons and related crystal properties from density-functional perturbation theory. *Rev. Mod. Phys.* **73**, 515–562 (2001).

[32] Giannozzi, P. *et al.* Quantum espresso: a modular and open-source software project for quantum simulations of materials. *J. Phys. Condens. Matter* **21**, 395502 (2009).

[33] Vanderbilt, D. Soft self-consistent pseudopotentials in a generalized eigenvalue formalism. *Phys. Rev. B* **41**, 7892–7895 (1990).

[34] Aroyo, M. I., Perez-Mato, J. M., Capillas, C., Kroumova, E., Ivantchev, S., Madariaga, G., Kirov, A. & Wondratschek, H. Bilbao crystallographic server: I. databases and crystallographic computing programs. *Zeitschrift für Kristallographie* **221**, 15–27 (2006).

[35] Aroyo, M. I., Kirov, A., Capillas, C., Perez-Mato, J. M. & Wondratschek, H. Bilbao Crystallographic Server. II. Representations of crystallographic point groups and space groups. *Acta Crystallographica Section A* **62**, 115–128 (2006).

[36] Cao, W. Phenomenological theories of ferroelectric phase transitions. *British Ceramic Transactions* **103**, 71–75 (2004).

[37] Perdew, J. P. & Zunger, A. Self-interaction correction to density-functional approximations for many-electron systems. *Phys. Rev. B* **23**, 5048–5079 (1981).

[38] Becke, A. D. Density-functional exchange-energy approximation with correct asymptotic behavior. *Phys. Rev. A* **38**, 3098–3100 (1988).

[39] Lee, C., Yang, W. & Parr, R. G. Development of the Colle-Salvetti correlation-energy formula into a functional of the electron density. *Phys. Rev. B* **37**, 785–789 (1988).

[40] Stroppa, A. & Kresse, G. The shortcomings of semi-local and hybrid functionals: what we can learn from surface science studies. *New Journal of Physics* **10**, 063020 (2008).

Extended Data Table I. **Birch-Murnaghan fit to the equation of state.** Parameters of the $P(V) = \frac{3}{2}B_0\left[(V_0/V)^{7/3} - (V_0/V)^{5/3}\right]\left[1 + \frac{3}{4}(B_0' - 4)[(V_0/V)^{2/3} - 1]\right]$ fit to the equation of state for $Im\bar{3}m$ with classical nuclei, and with vibrational contributions for both H_3S and D_3S.

	B_0 (GPa)	V_0 (a_0^3)	B_0'
Classical nuclei	129.8	158.4	3.6
H_3S	86.63	176.4	3.9
D_3S	87.81	174.8	3.9

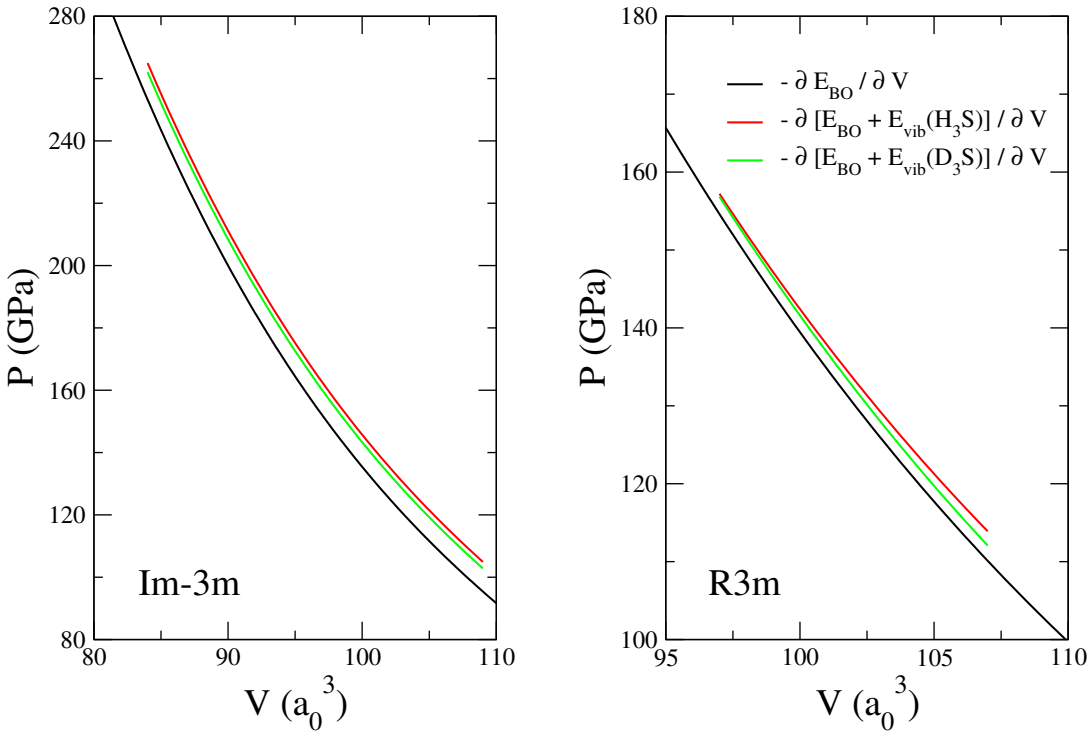

Extended Data Figure 1. **Equations of state.** Pressure as a function of volume calculated from the static energy E_{BO} that represents the classical nuclei limit as well as including the vibrational contribution within the SSCHA for both H_3S and D_3S.

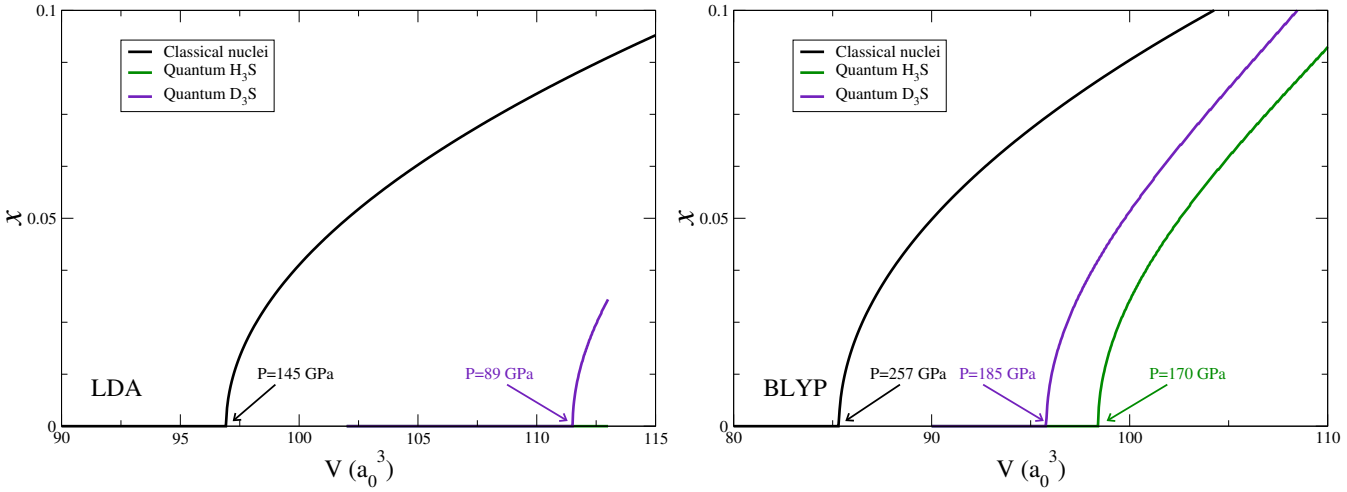

Extended Data Figure 2. **Bond symmetrization within LDA and BLYP.** For each volume the relative coordinate $x = (d_2 - a/2)/(a/2)$, where d_2 is the length of the hydrogen bond and a is the lattice parameter, obtained at the energy minimum is marked. When $x = 0$ the covalent and hydrogen bond have the same length and the structure is fully symmetric. The energy is calculated at the static level without any vibrational contribution as derived from the BOES, and including the quantum anharmonic vibrational contribution both for H_3S and D_3S. The pressure below which the cubic structure distorts is given in each case.

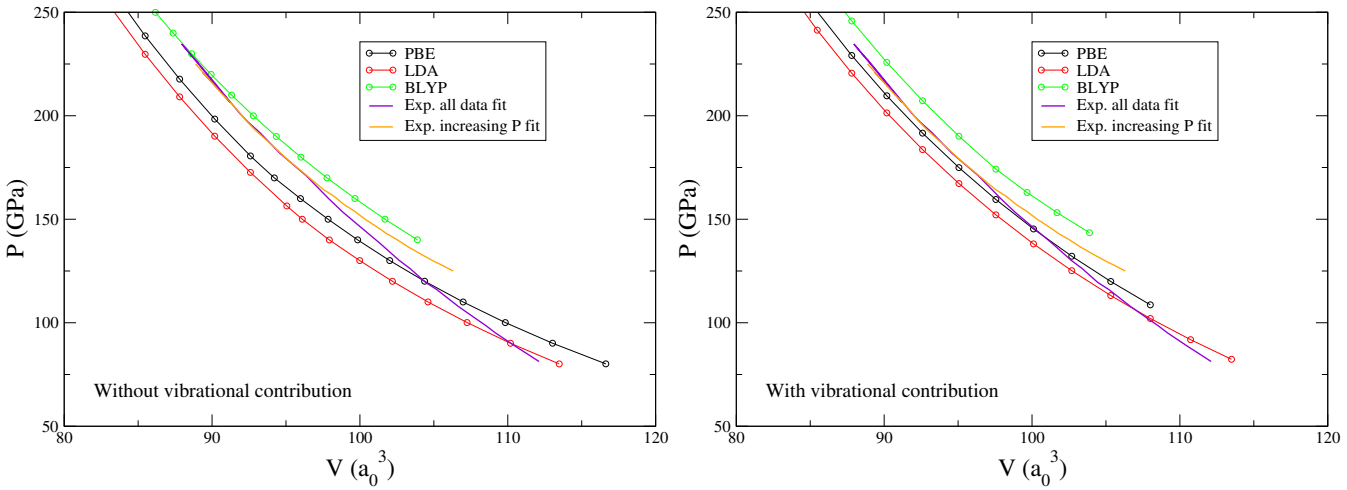

Extended Data Figure 3. **Functional dependence of the equation of state.** The equation of state is calculated with different exchange correlation functionals with and without the vibrational contribution to the pressure. At each volume the pressure of the structure with minimum energy is given, which depends on whether or not the vibrational contribution is included (see Extended Data Fig. 2). The results are compared with the two curves obtained experimentally [10].

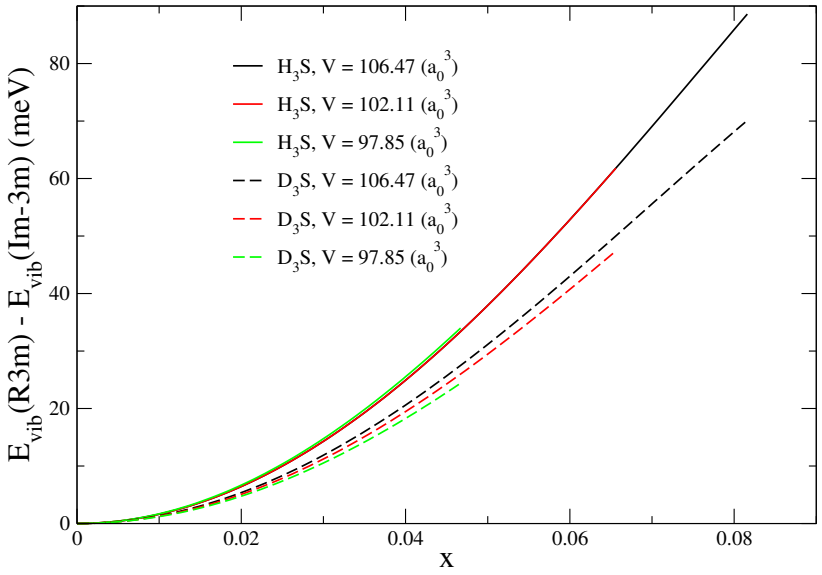

Extended Data Figure 4. **Vibrational energy.** SSCHA anharmonic vibrational energy calculated as a function of the relative coordinate $x = (d_2 - a/2)/(a/2)$ for different volumes.

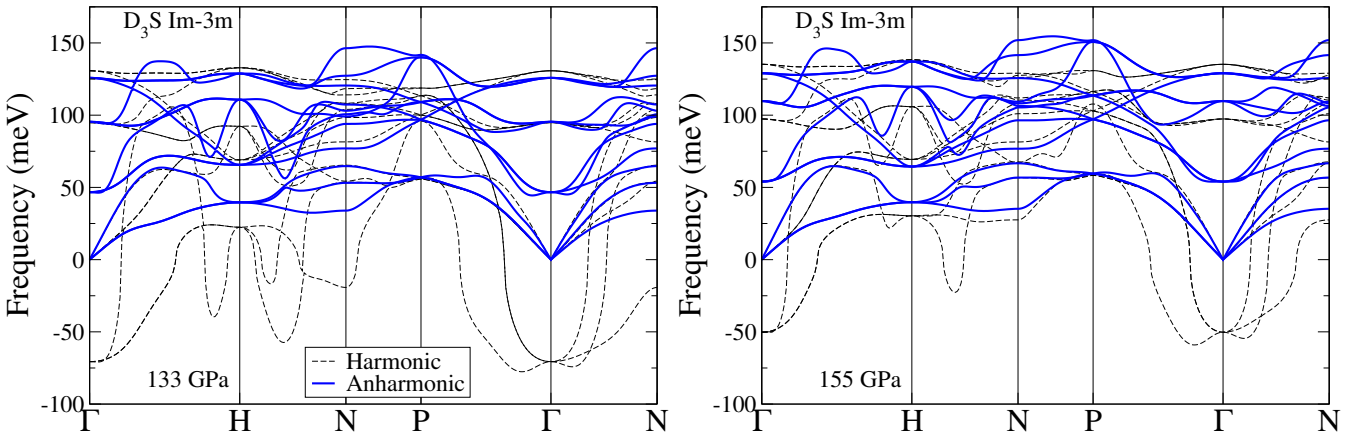

Extended Data Figure 5. **Phonons of $Im\bar{3}m$-D_3S.** Comparison between the harmonic and anharmonic phonons of $Im\bar{3}m$ at two different pressures for D_3S.

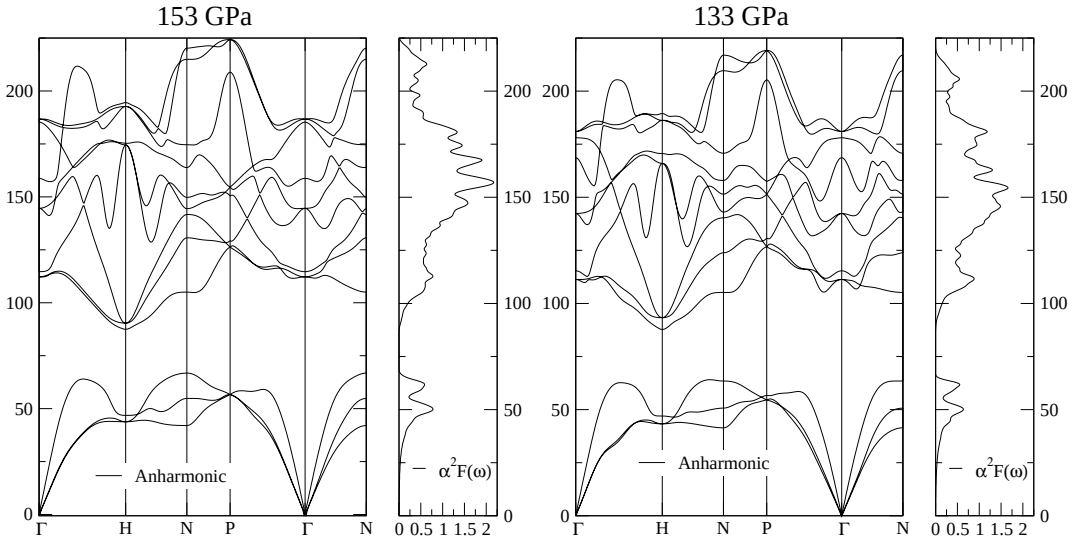

Extended Data Figure 6. **Anharmonic phonons of $R3m$-H_3S at two different pressures.** The Eliashberg functions $\alpha^2F(\omega)$ are also shown.

Extended Data Table II. **Raman and infrared active modes.** Phonon modes at the Γ point for the $Im\bar{3}m$ and $R3m$ phases at different pressures calculated including anharmonicity within the SSCHA. The results for $R3m$ are obtained keeping the centroid position at the minimum of the BOES. Raman (R) and Infrared (I) activity is indicated for each mode.

$Im\bar{3}m$						
Mode	Degeneracy	R or I active?	ω (meV)			
			H_3S		D_3S	
			135 GPa	157 GPa	133 GPa	155 GPa
T_{1u}	3	I	79.6	87.6	46.7	54.1
T_{1u}	3	I	131.0	152.1	95.4	109.8
T_{2u}	3		177.3	182.0	125.8	129.0
$R3m$						
Mode	Degeneracy	R or I active?	ω (meV)			
			H_3S		D_3S	
			133 GPa	153 GPa	133 GPa	153 GPa
E	2	R+I	111.3	112.2	74.4	73.7
A_1	1	R+I	115.4	114.7	79.8	73.7
E	2	R+I	142.4	144.6	105.6	105.9
A_1	1	R+I	168.7	158.8	123.2	115.0
A_2	1		178.0	185.3	125.1	130.7
E	2	R+I	181.0	186.7	127.0	131.7

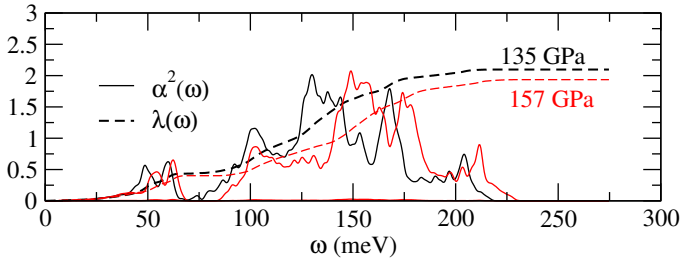

Extended Data Figure 7. **Superconducting properties of $Im\bar{3}m$-H_3S.** Anharmonic Eliashberg function $\alpha^2F(\omega)$ and integrated electron-phonon coupling constant $\lambda(\omega)$ of the $Im\bar{3}m$ phase at two different pressures.

Extended Data Table III. **Superconducting parameters.** Calculated λ, $\omega_{\log}$ and T_c. The pressure given includes the vibrational contribution.

	Compound	P (GPa)	λ	$\omega_{\log}$(meV)	T_c (K)
SSCHA $Im\bar{3}m$					
	H_3S	135	2.10	104.9	214
	H_3S	157	1.94	113.8	216
	D_3S	133	2.45	70.5	163
	D_3S	155	2.08	82.9	163
SSCHA $R3m$					
	H_3S	133	1.62	105.8	163
	H_3S	153	1.93	109.3	205
	D_3S	132	1.64	79.8	123
	D_3S	152	2.00	81.4	155